

## Aeolian Transport Layer

Murilo P. Almeida, José S. Andrade, Jr., and Hans J. Herrmann\*

*Departamento de Física, Universidade Federal do Ceará, 60455-900 Fortaleza, Ceará, Brazil*  
(Received 29 April 2005; revised manuscript received 23 September 2005; published 6 January 2006)

We investigate the airborne transport of particles on a granular surface by the saltation mechanism through numerical simulation of particle motion coupled with turbulent flow. We determine the saturated flux  $q_s$  and show that its behavior is consistent with classical empirical relations obtained from wind tunnel measurements. Our results also allow one to propose and explain a new relation valid for small fluxes, namely,  $q_s = a(u_* - u_t)^\alpha$ , where  $u_*$  and  $u_t$  are the shear and threshold velocities of the wind, respectively, and the scaling exponent is  $\alpha \approx 2$ . We obtain an expression for the velocity profile of the wind distorted by the particle motion due to the feedback and discover a novel dynamical scaling relation. We also find a new expression for the dependence of the height of the saltation layer as a function of the wind velocity.

DOI: [10.1103/PhysRevLett.96.018001](https://doi.org/10.1103/PhysRevLett.96.018001)

PACS numbers: 45.70.Mg, 47.27.-i, 47.55.Kf, 83.80.Hj

The transport of sand by wind is a major factor in sand encroachment, dune motion, and the formation of coastal and desert landscapes. The dominating transport mechanism is saltation as first described by Bagnold [1], which consists of grains being ejected upwards, being accelerated by the wind, and finally impacting onto the ground producing a splash of new ejected particles. Reviews are given in Refs. [2,3]. Quantitatively this process is, however, far from being understood.

Because of Newton's second law, the wind loses more momentum with increasing number of airborne particles until a saturation is reached. The maximum number of grains a wind of given strength can carry through a unit area per unit time defines the saturated flux of sand  $q_s$ . This quantity has been measured by many authors in wind tunnel experiments and on the field, and numerous empirical expressions for its dependence on the strength of the wind have been proposed [4–9]. In previous studies theoretical forms have also been derived using approximations for the drag in turbulent flow [10,11]. All these relations are expressed as polynomials in the wind shear velocity  $u_*$  which are of third order, under the assumption that the grain hopping length scales with  $u_*$  [4,5,10–12] and otherwise can be more complex [6]. The velocity profile in a particle laden layer has also been the object of measurement [13,14] and modelization [15]. Surprisingly, however, very few measurements of the height of the saltation layers as a function of  $u_*$  have been reported [16], and no systematic data close to the threshold are available. The complete analytical treatment of this problem remains out of reach not only because of the turbulent character of the wind, but also because of the underlying moving boundary conditions in the equations of motion. More recently, a deterministic model for aeolian sand transport without height dependency in the feedback has been proposed [17] in which grains of high (saltons) and low (reptons) energy coexist. Despite much research in the past [18], there remain many uncertainties about the trajectories of

the particles and their feedback with the velocity field of the wind. It is this challenge that motivated the present work and led us to discover a scaling relation for the distortion of the velocity profile.

We present the first numerical study of saltation that solves the turbulent wind field and its feedback with the dragged particles. As compared to real data, our values have no experimental fluctuations either in the wind field or in the particle size. As a consequence, we can determine all quantities with higher precision than ever before, and therefore with a better resolution close to the critical velocity at which the saltation process starts.

In order to get quantitative understanding of the layer of airborne particle transport above a granular surface, we simulate the situation inside a two-dimensional channel with a mobile top wall as schematically shown in Fig. 1. We impose a pressure gradient between the left and the right sides. Gravity points down, i.e., in the negative  $y$  direction. The  $y$  dependence of the pressure drop is adjusted in such a way as to ensure a logarithmic velocity profile along the entire channel in the case without particles, as it is expected in fully developed turbulence [19]. More precisely, this profile follows the classical form

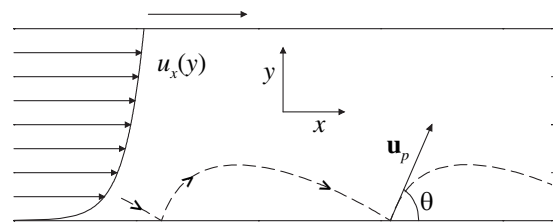


FIG. 1. Schematic representation of the setup showing the mobile wall at the top, the velocity field at different positions in the  $y$  direction, and the trajectory of a particle stream (dashed line). At the collision between this stream and the static wall at the bottom, we consider that the particles rebound to the air flow at an ejection angle  $\theta$ , with only a fraction  $r$  of their original kinetic impact energy.

$$u_x(y) = (u_*/\kappa) \ln(y/y_0), \quad (1)$$

where  $u_x$  is the component of the wind velocity in the  $x$  direction,  $u_*$  is the shear velocity,  $\kappa = 0.4$  is the von Karman constant, and  $y_0$  is the roughness length that is typically between  $10^{-4}$  and  $10^{-2}$  m. The upper wall of the channel is moved with a velocity equal to the velocity of the wind at that height in order to ensure a nonslip boundary condition.

The fluid mechanics inside the channel is based on the assumptions that we have an incompressible and Newtonian fluid flowing under steady-state and homogeneous turbulent conditions. The fluid is air with viscosity  $\mu = 1.7894 \times 10^{-5} \text{ kg m}^{-1} \text{ s}^{-1}$  and density  $\rho = 1.225 \text{ kg m}^{-3}$ . The Reynolds-averaged Navier-Stokes equations with the standard  $k - \epsilon$  model are used to describe turbulence. The numerical solution for the velocity and pressure fields is obtained through discretization by means of the control volume finite-difference technique [20,21]. The integral version of the governing equations is considered at each cell of the numerical grid to generate a set of nonlinear algebraic equations that are pseudolinarized and solved. The criteria for convergence used in the simulations are defined in terms of residuals, i.e., a measure of the degree to which the conservation equations are satisfied throughout the flow field. In our simulations convergence is achieved only when each of the normalized residuals falls below  $10^{-6}$ .

After having produced a steady-state turbulent flow, we proceed with the simulation of the particle transport along the channel. Assuming that drag and gravity are the only relevant forces acting on the particles, their trajectory can be obtained by integrating the following equation of motion:

$$\frac{d\mathbf{u}_p}{dt} = F_D(\mathbf{u} - \mathbf{u}_p) + \mathbf{g}(\rho_p - \rho)/\rho_p, \quad (2)$$

where  $u_p$  is the particle velocity,  $\mathbf{g}$  is gravity, and  $\rho_p = 2650 \text{ kg m}^{-3}$  is a typical value for the density of sand particles. The term  $F_D(\mathbf{u} - \mathbf{u}_p)$  represents the drag force per unit particle mass where

$$F_D = \frac{18\mu}{\rho_p d_p^2} \frac{C_D \text{Re}}{24}, \quad (3)$$

$d_p = 2.5 \times 10^{-4}$  m is a typical particle diameter,  $\text{Re} \equiv \rho d_p |\mathbf{u}_p - \mathbf{u}|/\mu$  is the particle Reynolds number, and the drag coefficient  $C_D$  is taken from empirical relations [22]. Each particle in our calculation represents, in fact, a stream of real grains. It is necessary to take into account the feedback on the local fluid velocity due to the momentum transfer to and from the particles. Specifically, this coupling effect is considered here by alternately solving the discrete and continuous phase equations until the solutions in both phases agree. The momentum transfer from one phase to another is computed by adding the momentum

change of every particle as it passes through a control volume [21],

$$\mathbf{F} = \sum_{\text{particles}} F_D(\mathbf{u} - \mathbf{u}_p) \dot{m}_p \Delta t, \quad (4)$$

where  $\dot{m}_p$  is the mass flow rate of the particles and  $\Delta t$  the time step. The exchange term Eq. (4) appears as a sink in the continuous phase momentum balance.

In Fig. 1 we see the trajectory of one particle stream and the velocity vectors along the  $y$  direction. Each time a particle hits the ground it loses a fraction  $r$  of its energy, and a new stream of particles is ejected at that position with an angle  $\theta$ . The parameters  $r = 0.84$  and  $\theta = 36^\circ$  are chosen from experimental measurements [23,24]. We also studied other values for  $r$  and  $\theta$  and even considered a continuous distribution of ejection angles. As expected, the choice of unrealistic values produces unphysical results. More details will be given in Ref. [25].

If  $u_*$  is below a threshold value  $u_t$ , the energy loss at each impact prevails over the energy gain during the acceleration through drag and particle transport comes to a halt as illustrated in Fig. 2. Only for  $u_* > u_t$  is steady sand motion achieved. The resulting flux is given by

$$q = \dot{m}_p n_p, \quad (5)$$

where  $n_p$  is the number of particle streams released. The first added particle streams are strongly accelerated in the channel, and their jumping amplitude increases after each ejection until a maximum is reached as seen in Fig. 2. The more particles are injected the smaller is this final amplitude. Beyond a certain number  $n_p$  of particle streams, the trajectories, however, start to lose energy and the overall flux is reduced. This critical value  $n_p$  characterizes the saturated flux  $q_s$  through Eq. (5).

In Fig. 3 we see the plot of  $q_s$  as a function of the wind velocity  $u_*$ . Clearly, there exists a critical wind velocity threshold  $u_t$  below which no sand transport occurs at all. This agrees well with experimental observations [1,5]. Also shown in Fig. 3 is the best fit to the numerical data using the classical expression proposed by Lettau and Lettau [5],

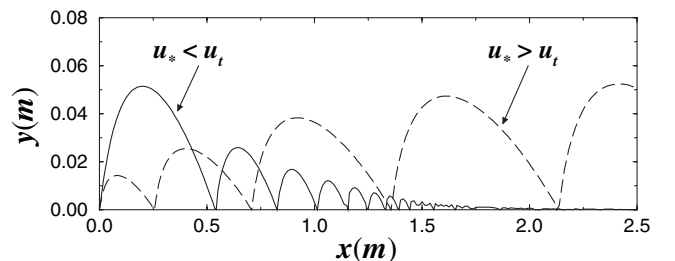


FIG. 2. Typical trajectories of particles computed for  $u_* < u_t$  (solid line) and  $u_* > u_t$  (dashed line).

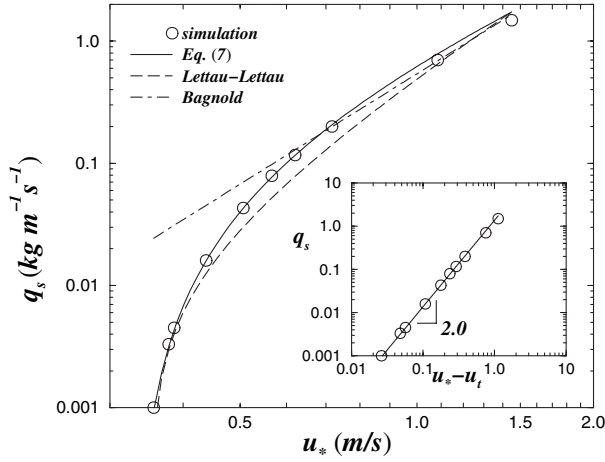


FIG. 3. Logarithmic plot of the saturated flux  $q_s$  as a function of  $u_*$ . The dashed line is the fit using the expression proposed by Lettau and Lettau [5],  $q_s \propto u_*^2(u_* - u_t)$ , with  $u_t = 0.35 \pm 0.02$ . The solid line corresponds to Eq. (7) and the dash-dotted line to Bagnold's relation,  $q_s \propto u_*^3$  [4]. The results shown in the inset confirm the validity of the power-law relation Eq. (7),  $q_s \propto (u_* - u_t)^2$ , with the critical point given by  $u_t = 0.33 \pm 0.01$ .

$$q_s = C_L \frac{\rho}{g} u_*^2 (u_* - u_t), \quad (6)$$

where  $C_L$  is an adjustable parameter. We find rather good agreement using fit parameters of the same order as those of the original work [5] and a threshold value of  $u_t = 0.35 \pm 0.02$ . This is, in fact, to our knowledge, the first time a numerical calculation is able to quantitatively reproduce this empirical expression, and it confirms the validity of our simulation procedure. Other empirical relations from the literature [10–12] can also be used to fit these results. In Fig. 3 we also show that for large values of  $u_*$  asymptotically one recovers Bagnold's cubic dependence. Close to the critical velocity  $u_t$  interestingly we find that a parabolic expression of the form

$$q_s = a(u_* - u_t)^2 \quad (7)$$

fits the data better than Eq. (7), as can be seen in Fig. 3 and, in particular, in the inset. The quadratic law of Eq. (7) can be understood by noticing that the shear stress at the ground should be decomposed into a dynamical and a turbulent part,  $\tau = \tau_d + \tau_T$ , the first being proportional to  $\eta u_*$  and the second proportional to  $\mu(u_* - u_t)$ , where  $\eta$  and  $\mu$  are the dynamical and the turbulent viscosities. In the limit  $u_* \gg u_t$  one obtains the classical behavior of Bagnold [4], as verified by the dash-dotted line in Fig. 3 and which is consistent with Refs. [5,10–12]. The limit  $u_* \approx u_t$ , however, yields the quadratic relation for the flux given in Eq. (7). Physically this is due to the fact that close to  $u_t$  the laminar component cannot be neglected.

The velocity profile of the wind within the layer of grain transport is experimentally much more difficult to access than the flux. This profile clearly deviates from the undis-

turbed logarithmic form of Eq. (1) because of the momentum the fluid must locally exchange with the particles. In Fig. 4 we show the loss of velocity with respect to the logarithmic profile without particles of Eq. (1) for different values of  $q$  as a function of the height  $y$ . As clearly seen in Fig. 4, the loss of velocity is maximal at the same height  $y_{\max}$ , regardless of the value of flux  $q$ . Except for large values of the flux, dividing the velocity axis by  $q$  one can collapse all the profiles quite well on top of each other, as can be verified in the inset of Fig. 4.

The position  $y_{\max}$  of the height of maximum loss depends essentially linearly on  $u_*$  as shown in Fig. 5. This is consistent with the observation that the saltation jump length is proportional to  $u_*$  [11]. The proportionality constant obtained from the best linear fit to the data is 0.35 s. Quantitatively the data in Fig. 5 also fit very well into the experiment data plots of Ref. [16] and are consistent with the analytical arguments of Ref. [11]. By extrapolation to  $y_{\max} = 0$ , we obtain an alternative estimate for the threshold velocity,  $u_t = 0.35$  m/s, that is consistent with the values calculated before from the fits to the data using Eqs. (6) and (7).

Whoever has been in the desert or on a beach during a very windy day knows that the saltation process in nature looks like a sheet of particles floating above ground at a certain height  $y_s$ , which strongly depends on the wind velocity. This height corresponds to the position of the largest likelihood to find a particle as obtained from the maximum of the density profile of particles as a function of height  $y$ . Figure 5 implies that the profile of velocity difference of the wind has a minimum at a similar height, which is consistent with the maximal loss of momentum. Within the error bars our results, in fact, yield that  $y_s$

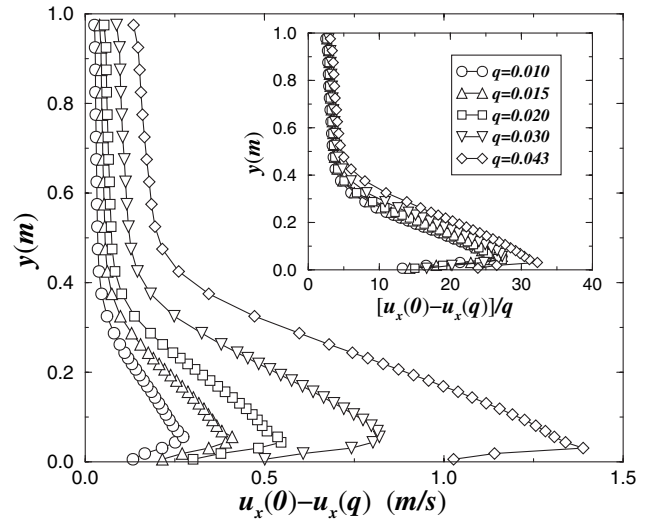


FIG. 4. Profile of the velocity difference  $u_x(0) - u_x(q)$  for different values of the flux  $q$  at  $u_* = 0.51$ . The inset shows the data collapse of these data obtained by rescaling the velocity difference with the corresponding  $q$ .

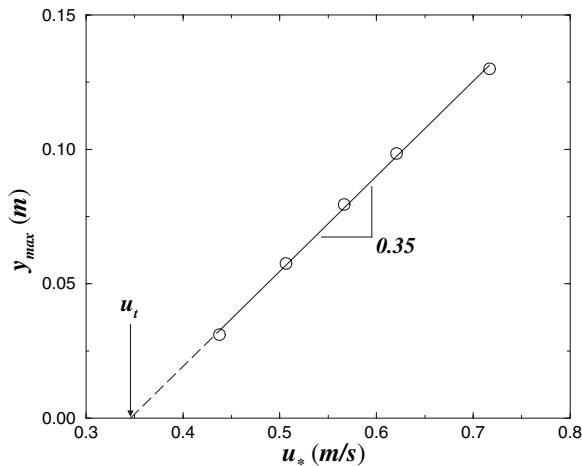


FIG. 5. Height  $y_{\max}$  of the maximum loss of velocity as a function of  $u_*$ . The height  $y_s$  of the largest probability to find a particle coincides with  $y_{\max}$ . The solid line corresponds to the best linear fit to the data with a slope equal to 0.35. By extrapolation, the intercept with the  $x$  axis provides an alternative estimate for the critical point,  $u_t = 0.35$  m/s, that is consistent with the other calculations.

coincides with the values of  $y_{\max}$  in Fig. 5. It is important to note that both heights,  $y_{\max}$  and  $y_s$ , also have the same linear dependence on  $u_*$ .

We have shown in this Letter results of simulations giving insight about the layer of granular transport in a turbulent flow. The lack of experimental noise allows for a precise study close to the critical threshold velocity  $u_t$  that leads us to a parabolic dependence of the saturated flux. In addition, we show that the velocity profile disturbed by the presence of grains scales linearly with the flux of grains, except close to saturation. Notably a characteristic height appears at which the momentum loss in the fluid and the grain density are maximized. Moreover, this height increases linearly with the wind velocity  $u_*$ . The present model can be extended in many ways including the study of the dependence of the aeolian transport layer on the grain diameter, the gas viscosity, and the solid or fluid densities. This would allow one to calculate, for instance, the granular transport on Mars and compare with the expression presented in Ref. [12]. Work in this direction is under way [25].

We thank Keld Rasmussen, Eric Parteli, Josué Mendes Filho, and Ascânio Dias Araújo for discussions and CNPq, CAPES, FUNCAP, FINEP, and the Max-Planck Institute for financial support.

\*Also at Institute for Computer Physics, University of Stuttgart, Stuttgart, Germany.

Electronic address: hans@ica1.uni-stuttgart.de

- [1] R. A. Bagnold, *The Physics of Blown Sand and Desert Dunes* (Methuen, London, 1941).
- [2] R. S. Anderson, M. Sørensen, and B. B. Willetts, *Acta Mech. Suppl.* **1**, 1 (1991).
- [3] H. J. Herrmann, in *The Physics of Granular Media*, edited by H. Hinrichsen and D. Wolf (Wiley VCH, Weinheim, 2004), pp. 233–252.
- [4] R. A. Bagnold, *Proc. R. Soc. A* **167**, 282 (1938).
- [5] K. Lettau and H. Lettau, in *Exploring the World's Driest Climate*, edited by H. Lettau and K. Lettau (University of Wisconsin, Madison, 1978).
- [6] B. T. Werner, *J. Geol.* **98**, 1 (1990).
- [7] K. R. Rasmussen and H. E. Mikkelsen, *Acta Mech. Suppl.* **1**, 135 (1991).
- [8] Y.-H. Zhou, X. Guo, and X. J. Zheng, *Phys. Rev. E* **66**, 021305 (2002).
- [9] J. D. Iversen and K. R. Rasmussen, *Sedimentology* **46**, 723 (1999).
- [10] P. R. Owen, *J. Fluid Mech.* **20**, 225 (1964).
- [11] M. Sørensen, in *Proceedings of the International Workshop on Physics of Blown Sand* (University of Aarhus, Denmark, 1985), Vol. 1, p. 141; *Acta Mech. Suppl.* **1**, 67 (1991).
- [12] B. R. White, *Geophys. Res.* **84**, 4643 (1979).
- [13] G. R. Butterfield, in *Turbulence: Perspectives on Flow and Sediment Transport*, edited by N. J. Clifford, J. R. French, and J. Hardisty (John Wiley, New York, 1993), Chap. 13, p. 305.
- [14] K. Nishimura and J. C. R. Hunt, *J. Fluid Mech.* **417**, 77 (2000).
- [15] J. E. Ungar and P. K. Haff, *Sedimentology* **34**, 289 (1987).
- [16] Z. Dong, X. Liu, H. Wang, A. Zhao, and X. Wang, *Geomorphology* **49**, 219 (2003).
- [17] B. Andreotti, *J. Fluid Mech.* **510**, 47 (2004).
- [18] P. Nalpanis, J. C. R. Hunt, and C. F. Barrett, *J. Fluid Mech.* **251**, 661 (1993).
- [19] L. Prandtl, in *Aerodynamic Theory*, edited by W. F. Durand (Springer, Berlin, 1935), Vol. III, p. 34.
- [20] S. V. Patankar, *Numerical Heat Transfer and Fluid Flow* (Hemisphere, Washington, DC, 1980).
- [21] The FLUENT (trademark of FLUENT Inc.) commercial package for fluid dynamics analysis is used in this study.
- [22] S. A. Morsi and A. J. Alexander, *J. Fluid Mech.* **55**, 193 (1972).
- [23] R. S. Anderson and P. K. Haff, *Science* **241**, 820 (1988).
- [24] F. Rioual, A. Valance, and D. Bideau, *Phys. Rev. E* **62**, 2450 (2000).
- [25] M. P. Almeida, J. S. Andrade, Jr., and H. J. Herrmann (to be published).